

Article

Lidar Observations of the Fe Layer in the Mesopause and Lower Thermosphere over Beijing (40.5° N, 116.0° E) and Mohe (53.5° N, 122.4° E)

Kexin Wang ^{1,2} , Zelong Wang ^{1,2,*}, Yuxuan Wu ^{1,2}, Lifang Du ^{2,*}, Haoran Zheng ², Jing Jiao ², Fang Wu ² , Yuchang Xun ³  and Yuan Xia ⁴

¹ School of Science, Jiangsu University of Science and Technology, Zhenjiang 212100, China; wang.kexin@stu.just.edu.cn (K.W.)

² State Key Laboratory of Space Weather, National Space Science Center, Chinese Academy of Sciences, Beijing 100190, China

³ College of Physics, Taiyuan University of Technology, Taiyuan 030024, China

⁴ School of Electronic Engineering, Nanjing Xiaozhuang University, Nanjing 211171, China

* Correspondence: zlwang@just.edu.cn (Z.W.); lfd@nssc.ac.cn (L.D.)

Abstract: Lidar observations of metal layers play a significant role in research on the chemistry and dynamics of the mesosphere and lower thermosphere. This work reports on Fe lidar observations conducted in Beijing and Mohe. Utilizing the same laser emission system, a 1064 nm seed laser was injected into an Nd: YAG laser to generate a single longitudinal-mode pulse 532 nm laser, which pumped a dye laser to produce a 572 nm laser. The 572 nm laser and the remaining 1064 nm fundamental frequency laser passed through a sum-frequency module to generate a 372 nm laser to detect the Fe layer. According to a total of 52.6 h of observations for 10 nights in Beijing, the Fe layer has an average column density of $1.24 \times 10^{10} \text{ cm}^{-2}$, an RMS width of 4.4 km and a centroid altitude of 89.4 km. In Mohe, observed for 16 nights and a total of 91.5 h, the Fe layer has an average column density of $1.08 \times 10^{10} \text{ cm}^{-2}$, an RMS width of 4.6 km and a centroid altitude of 89.5 km. The probability of the occurrence of sporadic Fe layers was 42.4% in Beijing and 29.4% in Mohe. Compared to simultaneously observed Na layers, the occurrence probabilities of sporadic Fe layers were higher than those of sporadic Na layers in both stations. Based on the two cases observed in Beijing, it is conjectured that the formation mechanism of sporadic metal layers above approximately 100 km has a more significant influence on sporadic Fe layers than on sporadic Na layers. The lower thermospheric Fe layers with densities significantly larger than those of the main layer were observed during two nights in Mohe. This work contributes to the refinement of the global distribution of Fe layers and provides abundant observational data for the modeling and study of the metal layers.

Keywords: Fe lidar; mesosphere and lower thermosphere; sporadic Fe layers; lower thermospheric Fe layers



Citation: Wang, K.; Wang, Z.; Wu, Y.; Du, L.; Zheng, H.; Jiao, J.; Wu, F.; Xun, Y.; Xia, Y. Lidar Observations of the Fe Layer in the Mesopause and Lower Thermosphere over Beijing (40.5° N, 116.0° E) and Mohe (53.5° N, 122.4° E). *Atmosphere* **2024**, *15*, 344. <https://doi.org/10.3390/atmos15030344>

Academic Editor: Yuichi Otsuka

Received: 7 February 2024

Revised: 28 February 2024

Accepted: 11 March 2024

Published: 12 March 2024



Copyright: © 2024 by the authors. Licensee MDPI, Basel, Switzerland. This article is an open access article distributed under the terms and conditions of the Creative Commons Attribution (CC BY) license (<https://creativecommons.org/licenses/by/4.0/>).

1. Introduction

The mesosphere and lower thermosphere (MLT) is the region of the atmosphere from 50 to 120 km above the Earth's surface. Meteors and extraterrestrial dust are injected into the Earth's atmosphere and then ionize, ablate or sputter to produce metal vapors that form metal layers covering the global atmosphere in the MLT [1,2]. The metal layers are composed of various species of metal atoms, ions and oxides. Now the detectable metal particles include Na [3–7], K [8,9], Fe [10–12], Ni [13,14], Ca [15,16], Mg [17], Ca⁺ [18,19] and Mg⁺ [20]. These metal particles serve as excellent tracers for studying the chemical and dynamic processes within the atmosphere in this region. The detection of these metal particles is primarily performed using photometry [21], airglow spectrometers [22], satellites and lidar, which is the main ground-based detection equipment due to its high temporal and spatial resolution.

Fe is one of the most abundant detectable elements in the metal layer. Granier first detected Fe by lidar at the 372 nm line for four nights at L'Observatoire de Haute Provence (OHP) (44° N, 6° E), France in 1989 [10]. In that report, the observation showed that the average column density of Fe was $3.6 \times 10^9 \text{ cm}^{-2}$ in November and $2.6 \times 10^9 \text{ cm}^{-2}$ in April, respectively. Bill observed and reported that the average column density of Fe at Urbana (40° N, 88° W) was $1.43 \times 10^{10} \text{ cm}^{-2}$ in 1990 [23]. In 2002, Chu conducted observations of the Fe layer at the geographic North Pole [24], obtaining an average column density of $1.23 \times 10^{11} \text{ cm}^{-2}$. The column density of Fe varies by up to two orders of magnitude in different regions. The significant differences in the average column densities of the Fe layer observed at different locations and times indicate the need for more observations to enhance the global dataset.

Sporadic Fe layers were first observed in Urbana, Illinois by Bill [23]. These sporadic layers are primarily distributed in the altitude range of 90 to 103 km. Wang et al. observed the double sporadic Fe layers at Wuhan (31° N, 114° E) [25]. They conjectured that the sporadic metal layers at different altitudes may result from the ablation of different meteors with different velocities. Gardner observed three sporadic events in Urbana and proposed that sporadic Fe layers were formed through the neutralization of Fe^+ in the associated sporadic E layers in 1993 [3]. Yi reported that the altitude and movement trajectory of sporadic Fe layers are similar to those of sporadic Na layers, indicating a close similarity in the formation mechanisms of sporadic Fe and Na layers [26,27]. But Alpers found that the overall occurrence rate and duration of sporadic Fe layers are both greater than those of sporadic Na layers [28]. It seems that the occasional non-coincidence of sporadic Fe and Na layers awaits more observations and further analysis.

In recent years, the detection precision of the metal layers has continuously improved with the development of higher-power lidar systems. Metal layers in the thermosphere have been observed by lidar. Chu reported the observation of thermosphere–ionosphere Fe and Na (TIFe and TINa) over McMurdo (77.8° S, 166.7° E) in 2011 [29]. It is indicated that Fe and Na can appear at 155 km and their motion processes show the presence of clear fast gravity waves. Xun reported the observation of thermospheric Na layers at two lidar stations separated by a linear distance of 237 km [30]. The concurrent observations conducted at two neighboring stations reveal that more than half of the thermospheric Na layers have a horizontal scale of less than 250 km. The various special phenomena that make up the formation mechanism of the thermospheric metal layers have invoked a great amount interest. Chu et al. developed a thermosphere–ionosphere Fe/ Fe^+ model to analyze the formation mechanism of the Fe layers in the polar thermosphere in 2017 [31]. However, this mechanism requires further observational data from different locations to be optimized.

Observations of Fe layers have been conducted primarily in mid-to-high latitude regions in North America, Europe and Antarctica. However, there is only one Fe lidar observation station in the middle latitude regions of East Asia [26]. Therefore, more observations need to be conducted in East Asia, especially in the mid-to-high latitude regions. This will provide observational data for the global distribution of Fe layers. The Chinese Meridian Project Phase II built a Fe resonance fluorescence lidar in Beijing (40.47° N, 115.97° E) in August 2022. The laser emission system was later moved to Mohe (53.5° N, 122.37° E) at the end of 2022 and observations were conducted in 2023.

This work reports the first lidar observations of the Fe layer conducted in Beijing (2022) and Mohe (2023). The results obtained for the Fe layer are compared with the global lidar measurements from other stations. The special phenomena related to the sporadic Fe layers and the lower thermospheric Fe layers are presented, which were also compared with the simultaneous observations of the Na layers. Additionally, the differences in their possible formation mechanisms are discussed in detail. This work contributes to having a comprehensive understanding of the Fe layer to advance our knowledge of the chemical and dynamic evolution characteristics in the mesosphere and lower thermosphere.

2. Instrument and Data

2.1. Lidar System

The Fe resonance fluorescence lidar systems used in this work were built by Chinese Meridian Project Phase II [2,32,33]. Both the Beijing and Mohe stations were configured using the same laser emission system which can generate a laser with a wavelength of 371.9937 nm in air. Figure 1 shows the complete schematic of the lidar system. In the laser emission system, the 1064 nm seed laser was controlled by the computer and injected into the YAG laser to generate a single longitudinal-mode pulse 532 nm laser. The remaining 1064 nm fundamental frequency laser was separated from the 532 nm pulse laser by the beamsplitter. The dye laser was pumped by the 532 nm laser to generate the 572 nm laser. Finally, the remaining 1064 nm laser and the 572 nm laser passed through a sum-frequency crystal module to generate a 371.9937 nm laser. The wavelength meter was connected to the computer to monitor the wavelength of the emission laser. The computer controlled the final emitted laser wavelength mainly by modifying the wavelength of the dye laser.

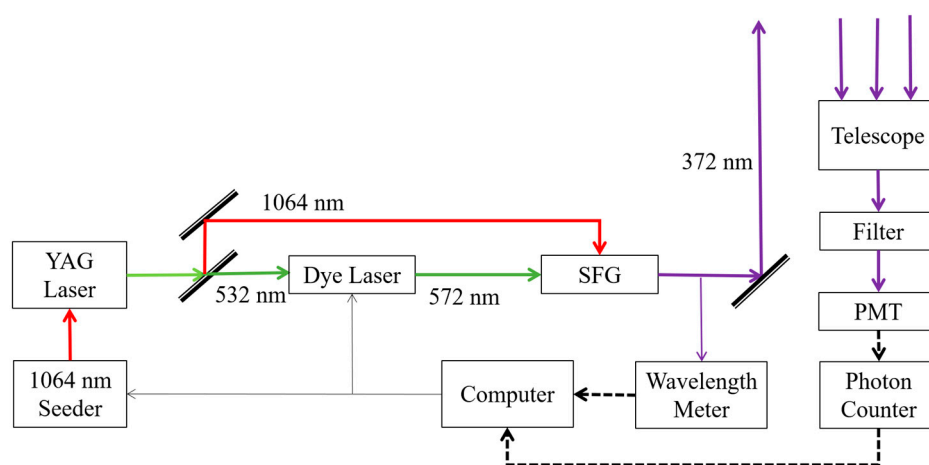


Figure 1. Schematic of the Fe lidar system. Different color arrows represent different wavelengths of lasers (red: 1064 nm, green: 532 nm and 572 nm, purple: 372 nm). The gray arrows indicate the signal control, and black dashed arrows indicate data transmission.

The receiver of the Fe lidar captures backscattered resonance fluorescence photons from the atmosphere through the telescopes with apertures of 1.2 m in Beijing and 1.5 m in Mohe, respectively. The raw photon signals from the filter were then converted into electrical signals and amplified by the photomultiplier tube (PMT). The amplified signals were counted and recorded by the photon counter. The recorded number of photons was processed and stored by the computer. Table 1 shows the main parameters of the two Fe lidar systems.

Table 1. Fe lidar system parameters in Beijing and Mohe.

	Beijing	Mohe
Location	40.47° N, 115.97° E	53.49° N, 122.34° E
Laser wavelength/nm	371.9937	371.9937
Pulse energy/mJ	~30	~30
Pulse width/ns	10	10
Repetition rate/Hz	30	30
Telescope diameter/m	1.2	1.5
Telescope Field of view/mrad	0.6	0.6
Optical filter Bandwidth/nm	1	1

2.2. Data Processing and Descriptions

The resonance fluorescence scattering cross-section is an important parameter for density inversion. In the calculation of the resonance fluorescence scattering cross section, both Doppler broadening and natural broadening of Fe were considered [34]. The Fe Doppler broadening was calculated to be 1.09 GHz under the assumption of the temperature of 200 K. The natural broadening was calculated to be 2.58 MHz. The center wavelength of the emitting laser was set to 371.9937 nm. A temperature of 200 K is usually assumed in the references when the resonance fluorescence cross sections of metal particles are calculated in the metal layers [11,16]. The peak absorption cross section of Fe was calculated to be $9.46 \times 10^{-17} \text{ m}^2$ at 200 K, which closely matches the figure obtained from reference [35]. It is necessary to consider the linewidth and lineshape of the laser when calculating the effective scattering cross section. The emitting laser has a linewidth of 2.7 GHz, which is the full width at half maximum. The lineshape of the emitting laser is assumed to be a Gaussian shape. The effective backscattering cross-section of Fe at 371.9937 nm was calculated to be $2.82 \times 10^{-18} \text{ m}^2/\text{sr}$ at 200 K. This parameter was used in the data processing for the density inversion of the Fe atoms.

The photon counts obtained from the lidar system were used to invert the density of the Fe layer. Although the same emission system was utilized in both stations, differences exist in their respective receiving systems. The original temporal and spatial resolutions for Beijing and Mohe are 15 s and 96 m and 30 s and 32 m, respectively. Additionally, the telescope diameters are 1.2 m in Beijing and 1.5 m in Mohe. Figure 2 shows the original profiles of the photon counts observed in Beijing and Mohe between 30 to 120 km. The uncertainties of the Fe density are calculated based on the relative uncertainty caused by fluctuations in photon counts. Photon counts were collected with a temporal resolution of 15 min and a spatial resolution of 96 m to improve the SNR. The relative uncertainty of the lidar systems in Beijing and Mohe at the main peak were $\sim 0.9\%$ and $\sim 0.8\%$, respectively.

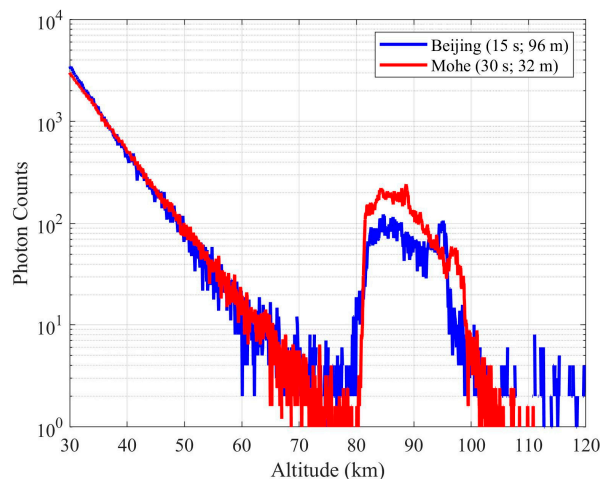


Figure 2. The raw photon counts observed in Beijing (Blue) at 16:20 on 19 August 2022, and in Mohe (Red) at 14:55 on 22 October 2023.

Observations of the Fe layers were conducted in Beijing in 2022 and Mohe in 2023. In Beijing, effective observations were conducted across 10 nights, accumulating a total duration of 52.6 h, and were concentrated in August, September, and November of 2022. In Mohe, the effective observations were conducted on 16 nights with a cumulative duration of 91.5 h. The observations were conducted in July, October, and November of 2023. The observational results for Beijing and Mohe are comprehensively showed in the next section.

3. Observational Results

3.1. Density Variations and Average Characteristics

The universal time and altitude distribution of Fe layers over Beijing and Mohe are shown in Figure 3. In this work, the lower boundary of the Fe layer is defined as the point where the Fe density drops to 15% of its peaks. As shown in Figure 3a, it can be seen that the lower boundary (white dashed line) of the Fe layer began to expand downward from 17:00. Then, the altitude of the lower boundary dropped to 77 km at 18:00 and existed persistently until the end of the observation. The peak density of the Fe layer during this night reached $3.2 \times 10^4 \text{ cm}^{-3}$. At the beginning of this night, the centroid height of the Fe layer was stable at 85 km. After 15:40, the centroid altitude gradually decreased to 83 km and remained at this altitude. Figure 3b shows the observation results for Mohe on 27 October 2023. The lower boundary of the Fe layer for this night was found at a height of 79 km at 13:00. Half an hour later, the lower boundary abruptly rose to 83 km, followed by a gradual descent at a vertical phase speed of 1.5 km/h. The lower boundary ceased its descent at 17:00. Then, the density of the Fe layer gradually decreased. Corresponding to the descent of the lower boundary, the centroid height of the Fe layer also exhibited a similar downward trend during the period from 13:30 to 17:00. A sporadic Fe layer appeared at 97 km and descended to 94 km between 14:10 and 16:50, exhibiting a vertical phase speed of 1.1 km/h. This demonstrates a dynamic trend similar with both the lower boundary and the centroid height.

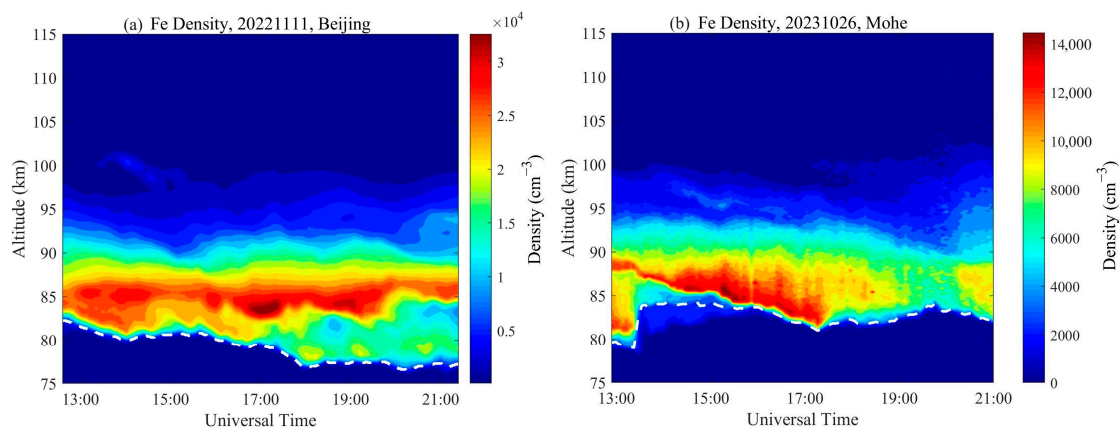


Figure 3. The density variations of the Fe layer. (a) Beijing on 11 November 2022; (b) Mohe on 26 October 2023. The white dashed lines are defined as the lower boundary of the main Fe layer.

Based on 10 nights of effective observations conducted in Beijing and 16 nights in Mohe, this work reported the average column density, RMS width, and centroid height of the Fe layer. Table 2 compared the average characteristics of the Fe layer in this work with other observations arranged from north to south. The observational results from Beijing are in close agreement with those from Urbana [23] and Boulder [36], which are located at the same latitude. However, the column density in Fort Collins at the same latitude is much smaller than those of the three locations. The average RMS width was around 4 km. The average centroid height ranged from approximately 88 km to 90 km, except for Andøya, which was 84.5 km. Although the observation time, lidar system and the background conditions are different in the comparisons, based on the limited measurements, it is difficult to find a direct correlation between the distribution characteristics of Fe layer and the latitude changes. The latitude of Mohe differs from existing observations. The observational results of Mohe are hard to compare with other stations. However, this observation filled the Fe layer observational gap between 50° N and 60° N in latitude.

Table 2. Comparisons of average characteristics of the Fe layers in Beijing, Mohe and other locations from north to south.

Location	Column Abundance ($\times 10^9 \text{ cm}^{-2}$)	Centroid Altitude (km)	RMS Width (km)	Peak Density ($\times 10^3 \text{ cm}^{-3}$)	Observation Time	References
North Pole	123.3				21 June 1999	Chu (2002) [24]
Andøya (69° N)	9.1	84.5		7.0	March 1990 to April 1990	Alpers (1990) [11]
Mohe (53.3° N)	10.8	89.5	4.6	18.2	July 2023 to November 2023	This Work
L'Observatoire de Haute Provence (49° N)	3.6 (Nov.); 2.6 (Apr.)				November 1986 and April 1987	Granier (1989) [10]
Beijing (40.5° N)	12.4	89.4	4.4	16.1	August 2022 to November 2022	This Work
Fort Collins (40.5° N)	2.4				July 9 1999	Chu (2002) [24]
Urbana (40° N)	14.3	89.4	3.8		October 1989	Bill (1990) [23]
Boulder (40° N)	10.7	89.7	4.4	13.0	August 2010 to September 2010	Huang (2011) [36]
Wuhan (30.5° N)	7.5	88.7	4.1	17.5	March 2004 to March 2005	Yi (2009) [37]
Kototabang (0.2° S)				2.0	24 June 2005	Nagasawa (2006) [38]
Rothera (67.5° S)	12.3	87.9	4.7		2002 to 2005	Gardner (2011) [39]
South Pole	9.7	88.4	4.2	4.3	December 1999 to October 2001	Gardner (2005) [40]

3.2. Sporadic Fe Layers Observed in Beijing and Mohe

The sporadic metal layer is typically characterized by a significant density enhancement structure floating over the main Fe layer. These layers commonly exhibit thicknesses between about 100 m and several kilometers [41]. The sporadic Fe layers observed in Beijing and Mohe are several kilometers in width. These layers were observed from 90 km to 110 km, displaying diverse structures. Some sporadic Fe layers exhibit a ribbon-like structure, persisting for a long duration (2 to 5 h) with a slow vertical phase speed during the observation period, as shown in Figure 4. It is noteworthy that, on some observational nights, independent double or triple sporadic Fe layers were observed simultaneously at different altitudes, clearly distinct from the main layer.

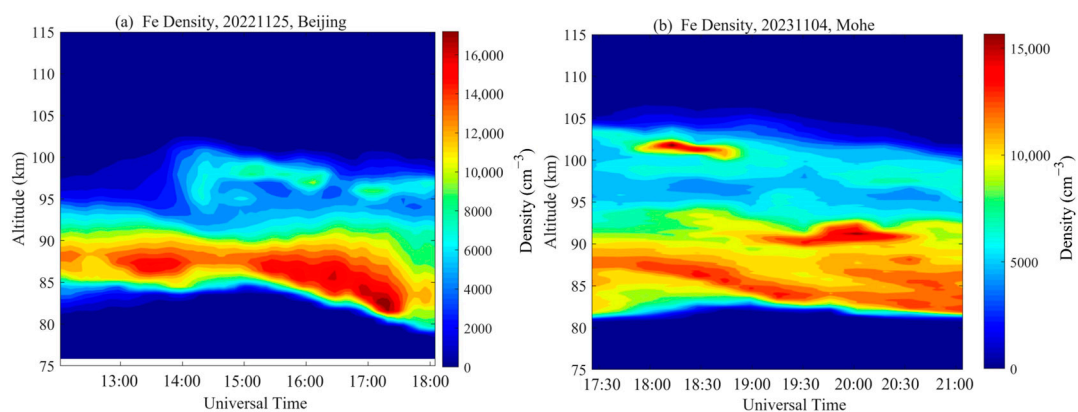
**Figure 4.** Sporadic Fe layers observed in (a) Beijing on 25 November 2022 and (b) Mohe on 4 November 2023.

Figure 4a shows the evolution of the sporadic Fe layer observed in Beijing on 25 November 2022. At the beginning of the observation, the upper boundary height of the main layer was 97 km. And 1.5 h later, it ascended to 102 km at 13:40. From then on, there was a sudden increase in Fe density at the altitudes from 93 to 101 km, forming a thick sporadic Fe layer detached from the main layer. Thirty minutes later, this sporadic Fe layer gradually narrowed, subsequently forming a double sporadic Fe layer at 95 km and 99 km. The higher sporadic layer at 99 km persisted until end of this night, with a density of about

8000 cm^{-3} . The lower sporadic layer at 95 km had a short duration and disappeared after 15:10. The higher sporadic layer at 99 km started its descent at 14:00 with a small vertical phase speed of 0.8 km/h, exhibiting a similar trend to the lower boundary of the main layer. But they descended at different vertical phase speeds. The lower boundary of the main layer was at 84 km at 15:00, descending to 78 km in the subsequent two hours at a vertical phase speed of 2 km/h.

Figure 4b shows the variation of the sporadic Fe layer observed in Mohe on 4 November 2023. A double sporadic Fe layers appeared at 17:30. The first layer appeared at 104 km with a peak density of $15,800 \text{ cm}^{-3}$, while the second layer appeared at 99 km with a peak density of merely one-third that of the first layer. A new sporadic layer gradually formed at 93 km at 18:00, which was superimposed on the main layer. This layer, in conjunction with the sporadic layers at 104 km and 99 km, constituted a triple sporadic layer in a short time. At 18:30, the first sporadic layer at 104 km merged with the second sporadic layer at 99 km, forming a sporadic layer with a thickness of approximately 5 km. This layer persisted throughout the entire night, gradually descending with a vertical phase speed of 1.6 km/h. The centroid altitude of the main layer also exhibits a similar descending trend, with a vertical phase speed of 1.5 km/h, close to the vertical phase speed of the first sporadic layer. This seemingly revealed some atmospheric wave processes. The sporadic layer at 93 km reached its peak density of $15,900 \text{ cm}^{-3}$ at 20:00 and gradually merged with the main layer after 20:30.

3.3. Fe Layers Observed in the Lower Thermosphere

The Fe layer in the thermosphere was first observed and reported by Chu et al. in 2011 in McMurdo in Antarctica (77.8° S , 166.7° E) [29]. The thermospheric Fe layer typically occurs at altitudes from 110 to 155 km. Fe layers with extremely large density in the lower thermosphere were observed on two nights during the observations in Mohe, both occurring at approximately 110 km. Figure 5 shows the density profile of the Fe layer at 18:00 on 9 July 2023. At this moment, the peak density of the lower thermospheric Fe layer at 110 km was $7.3 \times 10^4 \text{ cm}^{-3}$. It was about three times that of the main layer, which is around $2.3 \times 10^4 \text{ cm}^{-3}$. However, the RMS widths of the two layers are quite similar. Figure 5 also shows another event of the lower thermospheric Fe layer observed at 16:30 on 11 July 2023. The peak height of this layer was also around 110 km, with a peak density of $1.7 \times 10^4 \text{ cm}^{-3}$. Although the overall density on 11 July is much smaller than that on 10 July, the density of the thermospheric Fe layer on 11 July was four times that of the main layer, which was $3.8 \times 10^3 \text{ cm}^{-3}$. These two layers also had similar RMS widths. The densities of the lower thermospheric Fe layers observed on these two occasions were significantly greater than that of the main layer, yet their thicknesses were comparable to the main layer. The extremely large density of the lower thermospheric Fe layer observed on 9 July 2023 in Mohe was particularly remarkable.

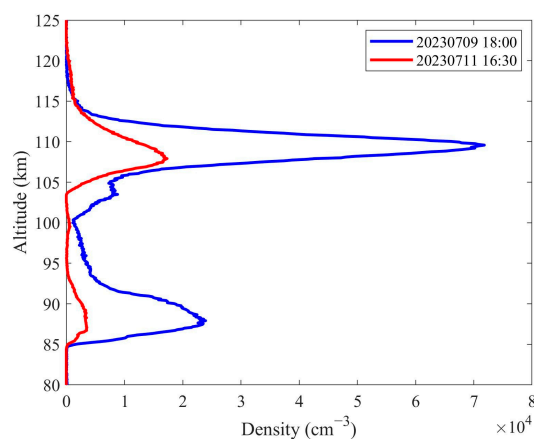


Figure 5. Two cases of the Fe layer observed in the lower thermosphere in Mohe.

4. Discussion

4.1. Comparison of Sporadic Fe and Na Layers

The sporadic Fe layers were compared with the simultaneously observed sporadic Na layer in both Beijing and Mohe in statistics. During the ten effective observational nights of Fe layer in Beijing, with a cumulative observation duration of 52.6 h, sporadic Fe layers were observed on nine nights, accumulating a total duration of 22.3 h. Based on the total duration of the sporadic Fe layer relative to the overall observation time, the occurrence probability of sporadic Fe layers in Beijing in autumn is approximately 42.4%. However, the cumulative observation duration of simultaneously observed sporadic Na layers at the same station was 48.5 h, and the observed duration of sporadic Na layers totaled 5.3 h, with an occurrence probability of approximately 10.9%. The occurrence probability of sporadic Fe layers observed in Beijing in autumn is approximately eight times greater than that of sporadic Na layers.

During the 16 effective observational nights of Fe layers in Mohe with a cumulative duration of 91.5 h, sporadic Fe layers were observed on 12 nights, accumulating a duration of 26.9 h. The total occurrence probability of sporadic Fe layers in Mohe is approximately 29.4%. The occurrence probability of sporadic metal layers depends on the seasons [42]. Specifically categorized by season, the occurrence probabilities of sporadic Fe layers were 74.8% in summer and 22.1% in autumn in Mohe, respectively. Simultaneous observations of Na layers were conducted for eight effective observational nights, with a total observation duration of 34.7 h. Among these, sporadic Na layers were observed on two nights in summer and one night in autumn, respectively. The total duration was 5.5 h, resulting in a total occurrence probability of approximately 15.9%. The occurrence probabilities of sporadic Na layers were 52.8% in summer and 6.2% in autumn, respectively. The occurrence probabilities of both sporadic Fe and Na layers in summer were higher than those in autumn in Mohe. The occurrence probabilities of sporadic Fe layers were about 1.5 times that of sporadic Na layers in summer and 3.6 times that in autumn in Mohe. For the same season in autumn, the occurrences probabilities of both sporadic Fe and Na layers in Mohe were lower than those in Beijing. Table 3 shows detailed statistical comparisons of the sporadic Fe layers and sporadic Na layers observed over Beijing and Mohe. It should be noted that, due to the debugging performed on the Na lidar, there are fewer observation times for the Na lidar than for the Fe lidar in Beijing and Mohe, which might lead to a slight discrepancy in the statistical results.

Table 3. Statistics of the sporadic Fe layers and sporadic Na layers in Beijing and Mohe.

	Beijing (Autumn)		Mohe (Summer)		Mohe (Autumn)	
	Fe	Na	Fe	Na	Fe	Na
Observation nights	10	8	5	3	11	5
Observation hours	52.6	48.5	12.7	7.2	78.8	27.5
Sporadic layer occurrence nights	9	2	5	2	7	1
Sporadic layer occurrence hours	22.3	5.3	9.5	3.8	17.4	1.7
Probability of occurrence in nights	90.0%	25.0%	100.0%	66.7%	63.6%	20.0%
Probability of occurrence in hours	42.4%	10.9%	74.8%	52.8%	22.1%	6.2%

The analysis of the results from both Beijing and Mohe indicate that the occurrence probability and duration of sporadic Fe layers are greater than those of sporadic Na layers. These contrasting results corroborate the conclusions drawn by Alpers in 1994 [28], who compared the individual characteristics of sporadic Fe layers and sporadic Na layers.

Figure 6a,b, respectively, show the density variations in Fe and Na observed simultaneously in Beijing on the night of 5 September 2022. The main Fe layer ranged from

83 km to 96 km. At 14:40, lower-density sporadic Fe layers appeared at 110 km, 105 km, and 100 km. At this time, the sporadic Fe layer at 110 km appeared, then descended to 107 km at 15:40. The sporadic Fe layers at 105 km and 100 km began to merge together at 15:00, before forming a new sporadic Fe layer located at 103 km by 15:30, with increasing density. At 16:10, the layer descended to 100 km, reaching 3000 cm^{-3} by 16:30. At 17:00, the sporadic Fe layer at 103 km suddenly extended downward, forming a new sporadic Fe layer at 96 km. They formed a triple sporadic Fe layer with the 107 km layer above them. The variation in the Na layer shows that between 15:40 and 17:20 sporadic structures are similar to the sporadic Fe layers formed at 101 km and 96 km, indicating a similar or identical formation mechanism for the sporadic Fe and Na layers appearing between 95 and 100 km [26,27]. More importantly, the presence of sporadic Fe layers was evident from 103 km to 110 km and persisted until the end of the observation, while no sporadic Na layer was observed at the same altitude and time.

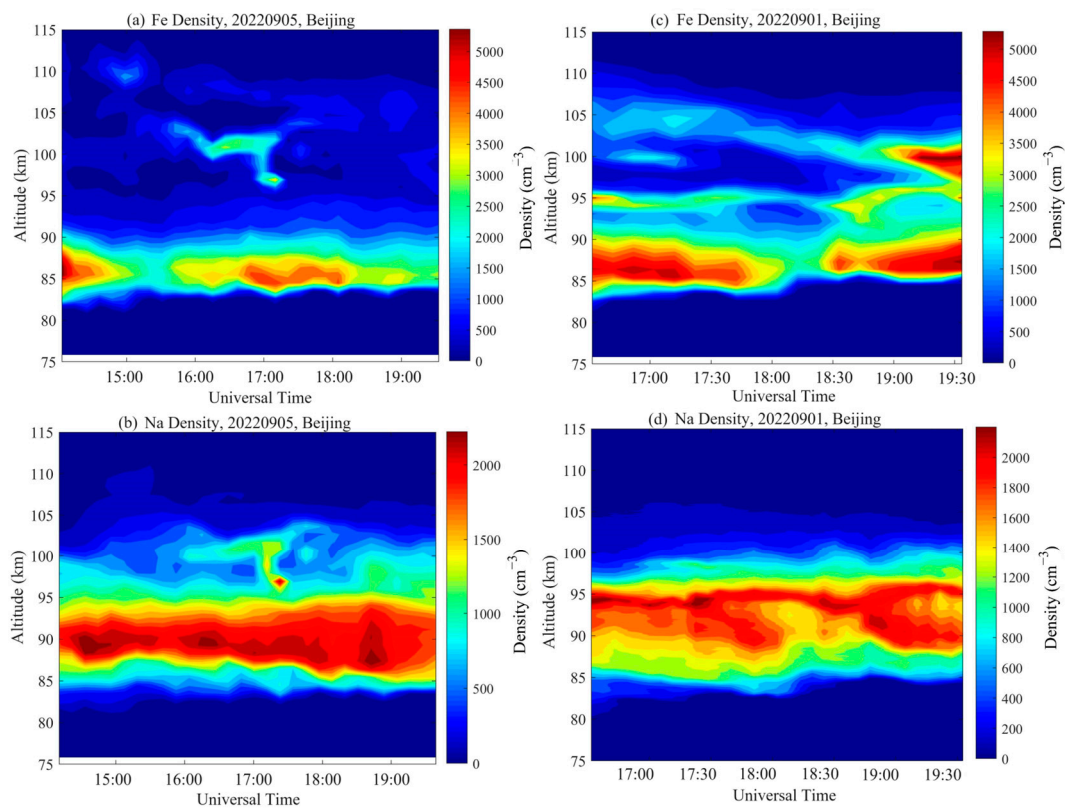


Figure 6. Comparisons of density variations in the Fe and Na layers observed in Beijing on 5 September 2022 (a,b) and on 1 September 2022 (c,d).

Figure 6c,d show the simultaneous observation of Fe and Na in Beijing on 1 September 2022. It was also found that the triple sporadic Fe layers were observed from 16:40 to 17:20. Their altitudes are located at 104 km, 100 km, and 95 km, respectively. The sporadic Fe layer at 104 km descended after 17:30, reaching 100 km by 19:00, with an increasing density that peaked at 5100 cm^{-3} , with a vertical phase speed of 1.2 km/h. The sporadic Fe layer at 100 km disappeared after 17:20. The lowest sporadic Fe layer maintained at an altitude of around 95 km, persisting until the end of the observation. A subtle sporadic Na layer was observed at 95 km, persisting throughout this night. By careful comparison, the structure and trajectory of this sporadic Na layer appear almost similar to the sporadic Fe layer at 95 km. This indicates that they shared a similar formation mechanism at this altitude. However, unlike the sporadic Fe layers which appeared above approximately 100 km, the sporadic Na layer was still absent above approximately 100 km, aligning with the findings from the observations made on 5 September 2022. For these two cases, in Figure 6, the

neutral dynamics, such as horizontal and vertical transport, play the same roles in the evolution processes of both Fe and Na layers. Therefore, the difference between the Fe and Na layers above 100 km is more likely due to the different chemical reaction processes in the atmosphere.

Yi et al. revealed that the sporadic Fe layers and sporadic Na layers always appeared at the same altitude with similar motion trajectories [26]. However, their discussion on the formation mechanism of sporadic layers mainly focused on the vicinity of the main layers. The results obtained in this work drew a similar conclusion below approximately 100 km, while they appear to deviate from that pattern above approximately 100 km. The occurrence probability of sporadic Fe layers is significantly higher than that of sporadic Na layers above approximately 100 km. This suggests a potential difference in the formation mechanisms of sporadic Fe layers and sporadic Na layers above approximately 100 km. Alternatively, the formation mechanism of sporadic layers above approximately 100 km have more influence on sporadic Fe layers than on sporadic Na layers, which needs further investigation.

4.2. Fe and Na Layers in the Lower Thermosphere

The lower thermospheric Fe and Na layers are compared in this section. The simultaneous observational results of Fe and Na in Mohe at 16:30 on 11 July 2023 are shown in Figure 7. As previously mentioned in Section 3.3, the lower thermospheric Fe layer was 4 times greater than that of the main layer. Concurrently, a Na layer was observed in the lower thermosphere with a peak density of about 500 cm^{-3} , also emerging at the altitude of 107 km. The peak density of the main Na layer was about $1.7 \times 10^3 \text{ cm}^{-3}$. The peak density of the thermospheric Na layer is only one-third of the peak density of the main Na layer. These observational results indicate that the formation mechanisms of Fe layers and Na layers in the lower thermosphere share similarities but exhibit distinctions.

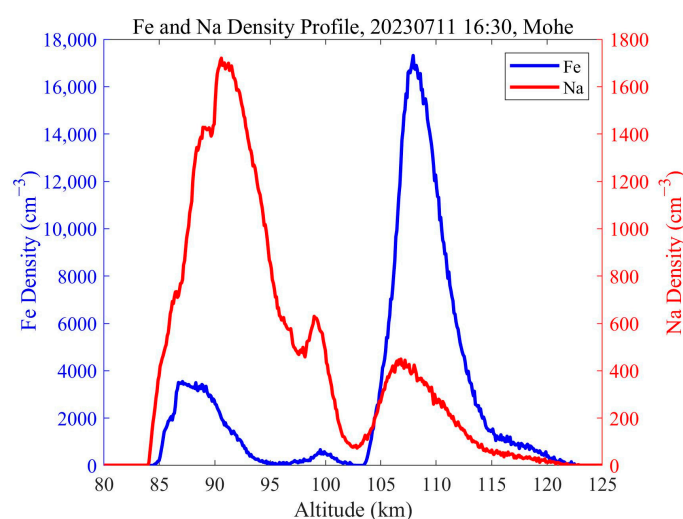


Figure 7. Comparison of the lower thermospheric Fe and Na layers simultaneously observed in Mohe at 16:30 on 11 July 2023.

Recent studies have indicated that the primary formation mechanism of Fe layers in the thermosphere is the in situ neutralization of Fe^+ [43]. The formation of the Na layer in the thermosphere is also considered to be produced by the in situ neutralization of converged Na^+ [44]. However, the neutralization rate of Na^+ is only one-third that of Fe^+ [45]. This seems to explain the much lower density of the thermospheric Na layer compared to the thermospheric Fe layer in this observation.

5. Conclusions

In this work, we conducted effective observations of the Fe layer for 10 nights in Beijing and 16 nights in Mohe, respectively. The average column density of Fe layers in

Beijing was $1.24 \times 10^{10} \text{ cm}^{-2}$, and the centroid height is 89.4 km. These observational results are highly consistent with those from Urbana and Boulder at the same latitude, but there is a significant difference compared to Fort Collins at the same latitude. The average column density of Fe layers in Mohe was $1.08 \times 10^{10} \text{ cm}^{-2}$ and the average centroid height is 89.4 km. The observation of Fe layers in Mohe filled the observational gap of Fe layers between 50° N and 60° N and expanded the global latitude distribution of Fe layer observations. Based on a comparison of the results from global observations, it can be seen that the global distribution of the Fe layer shows limited variations with latitudes.

Sporadic Fe layers were observed at both stations. The occurrence probability of sporadic Fe layers was 42.4% in Beijing and 29.4% in Mohe. These occurrence probabilities were significantly higher than those of sporadic Na layers simultaneously observed in both stations. The trend of sporadic Fe layers appearing more frequently than sporadic Na layers is similar with the simultaneous observation of Fe and Na at other stations.

Double and triple sporadic Fe layers were observed in both Beijing and Mohe. Based on two cases observed in Beijing, sporadic Fe layers were observed above about 100 km, while sporadic Na layers were either absent or not evident above this altitude. This suggests a potential difference in the formation mechanisms of sporadic Fe layers and sporadic Na layers above approximately 100 km. Alternatively, the formation mechanism of sporadic metal layers above that altitude has a more significant impact on the formation of sporadic Fe layers than that of sporadic Na layers.

In the observations in Mohe, lower thermospheric Fe layers were observed on two nights, with peak densities three to four times that of the main Fe layer. At the same altitude, the lower thermospheric Na layers were also observed, but their densities were only one-third of the main Na layer density. This result may be associated with the difference in the neutralization rates of Fe^+ and Na^+ ions.

The observations conducted in Beijing and Mohe filled a gap in Fe lidar observations of mid-to-high latitude regions in East Asia, which will contribute to the refinement of global Fe layer distribution. This work also provides valuable insights into the chemistry and dynamics of the Fe layer in Beijing and Mohe, and contributes to the broader understanding of metal layer in the mesosphere and lower thermosphere. In addition, it enhances our knowledge of the overall evolution process of the middle and upper atmosphere.

Author Contributions: Conceptualization, K.W., Z.W., Y.X. (Yuchang Xun) and L.D.; methodology, K.W., Z.W., Y.W., F.W. and L.D.; software, K.W. and Y.W.; validation, Y.X. (Yuan Xia), Y.X. (Yuchang Xun), F.W., J.J., H.Z. and L.D.; formal analysis, K.W., Y.W., Y.X. (Yuan Xia), Y.X. (Yuchang Xun) and L.D.; investigation, K.W., Y.W., F.W. and H.Z.; resources, Z.W., Y.X. (Yuan Xia), Y.X. (Yuchang Xun), J.J., H.Z. and L.D.; data curation, Z.W., L.D. and J.J.; writing—original draft preparation, K.W.; writing—review and editing, K.W., Z.W., Y.X. (Yuan Xia), Y.X. (Yuchang Xun), F.W., J.J., H.Z. and L.D.; visualization, K.W.; supervision, Z.W.; project administration, Z.W. and L.D.; funding acquisition, Z.W. All authors have read and agreed to the published version of the manuscript.

Funding: This research was funded by the Project of Collaborative Lidar Observation Experiment on Typical Stations.

Institutional Review Board Statement: Not applicable.

Informed Consent Statement: Not applicable.

Data Availability Statement: The original lidar data can be obtained from the Chinese Meridian Project (homepage: <https://data.meridianproject.ac.cn/> (accessed on 7 November 2023)).

Acknowledgments: The authors thank the reviewers for their instructions and suggestions and the editors for their help. The authors also acknowledge the use of data from the Chinese Meridian Project.

Conflicts of Interest: The authors declare no conflicts of interest. The funders had no role in the design of the study; in the collection, analyses, or interpretation of data; in the writing of the manuscript; or in the decision to publish the results.

References

1. Vondrak, T.; Plane, J.; Broadley, S.; Janches, D. A chemical model of meteoric ablation. *Atmos. Chem. Phys.* **2008**, *8*, 7015–7031. [[CrossRef](#)]
2. Wu, F.; Chu, X.; Du, L.; Jiao, J.; Zheng, H.; Xun, Y.; Feng, W.; Plane, J.M.; Yang, G. First Simultaneous Lidar Observations of Thermosphere-Ionosphere Sporadic Ni and Na (TISNi and TISNa) Layers (~105–120 km) Over Beijing (40.42° N, 116.02° E). *Geophys. Res. Lett.* **2022**, *49*, e2022GL100397. [[CrossRef](#)]
3. Gardner, C.S.; Kane, T.J.; Senft, D.C.; Qian, J.; Papen, G.C. Simultaneous observations of sporadic E, Na, Fe, and Ca⁺ layers at Urbana, Illinois: Three case studies. *J. Geophys. Res. Atmos.* **1993**, *98*, 16865–16873. [[CrossRef](#)]
4. Bills, R.E.; Gardner, C.S.; She, C.Y. Narrowband lidar technique for sodium temperature and Doppler wind observations of the upper atmosphere. *Opt. Eng.* **1991**, *30*, 13–21. [[CrossRef](#)]
5. Hu, X.; Yan, Z.; Guo, S.; Cheng, Y.; Gong, J. Sodium fluorescence Doppler lidar to measure atmospheric temperature in the mesopause region. *Chin. Sci. Bull.* **2011**, *56*, 417–423. [[CrossRef](#)]
6. Dou, X.; Qiu, S.; Xue, X.; Chen, T.; Ning, B. Sporadic and thermospheric enhanced sodium layers observed by a lidar chain over China. *J. Geophys. Res. Space Phys.* **2013**, *118*, 6627–6643. [[CrossRef](#)]
7. Cai, X.; Yuan, T.; Eccles, J.V.; Raizada, S. Investigation on the distinct nocturnal secondary sodium layer behavior above 95 km in winter and summer over Logan, UT (41.7 N, 112 W) and Arecibo Observatory, PR (18.3 N, 67 W). *J. Geophys. Res. Space Phys.* **2019**, *124*, 9610–9625. [[CrossRef](#)]
8. von Zahn, U.; Höffner, J. Mesopause temperature profiling by potassium lidar. *Geophys. Res. Lett.* **1996**, *23*, 141–144. [[CrossRef](#)]
9. Wang, Z.; Yang, G.; Wang, J.; Yue, C.; Yang, Y.; Jiao, J.; Du, L.; Cheng, X.; Chi, W. Seasonal variations of meteoric potassium layer over Beijing (40.41 N, 116.01 E). *J. Geophys. Res. Space Phys.* **2017**, *122*, 2106–2118. [[CrossRef](#)]
10. Granier, C.; Jégou, J.-P.; Mégie, G. Iron atoms and metallic species in the Earth's upper atmosphere. *Geophys. Res. Lett.* **1989**, *16*, 243–246. [[CrossRef](#)]
11. Alpers, M.; Höffner, J.; von Zahn, U. Iron atom densities in the polar mesosphere from lidar observations. *Geophys. Res. Lett.* **1990**, *17*, 2345–2348. [[CrossRef](#)]
12. Gardner, C.S.; Papen, G.C.; Chu, X.; Pan, W. First lidar observations of middle atmosphere temperatures, Fe densities, and polar mesospheric clouds over the North and South Poles. *Geophys. Res. Lett.* **2001**, *28*, 1199–1202. [[CrossRef](#)]
13. Collins, R.; Li, J.; Martus, C. First lidar observation of the mesospheric nickel layer. *Geophys. Res. Lett.* **2015**, *42*, 665–671. [[CrossRef](#)]
14. Gerding, M.; Daly, S.; Plane, J. Lidar soundings of the mesospheric nickel layer using Ni (3F) and Ni (3D) transitions. *Geophys. Res. Lett.* **2019**, *46*, 408–415. [[CrossRef](#)]
15. Granier, G.; Jégou, J.-P.; Mégie, G. Resonant lidar detection of Ca and Ca⁺ in the upper atmosphere. *Geophys. Res. Lett.* **1985**, *12*, 655–658. [[CrossRef](#)]
16. Alpers, M.; Höffner, J.; von Zahn, U. Upper atmosphere Ca and Ca⁺ at mid-latitudes: First simultaneous and common-volume lidar observations. *Geophys. Res. Lett.* **1996**, *23*, 567–570. [[CrossRef](#)]
17. Correia, J.; Aikin, A.; Grebowsky, J.; Pesnell, W.; Burrows, J. Seasonal variations of magnesium atoms in the mesosphere-thermosphere. *Geophys. Res. Lett.* **2008**, *35*, L06103. [[CrossRef](#)]
18. Gerding, M.; Alpers, M.; Von Zahn, U.; Rollason, R.; Plane, J. Atmospheric Ca and Ca⁺ layers: Midlatitude observations and modeling. *J. Geophys. Res. Space Phys.* **2000**, *105*, 27131–27146. [[CrossRef](#)]
19. Gerding, M.; Alpers, M.; Höffner, J.; Von Zahn, U. Sporadic Ca and Ca⁺ layers at mid-latitudes: Simultaneous observations and implications for their formation. *Ann. Geophys.* **2001**, *19*, 47–58. [[CrossRef](#)]
20. Yeh, S.-D.; Browell, E.V. Shuttle lidar resonance fluorescence investigations. 2: Analysis of thermospheric Mg⁺ measurements. *Appl. Opt.* **1982**, *21*, 2373–2380. [[CrossRef](#)]
21. Donahue, T.M.; Blamont, J.-E. Sodium in the upper atmosphere. In Proceedings of the Symposium d' Aéronomie Communications, Copenhagen, Denmark, 19–22 July 1960; International Union of Geodesy and Geophysics: Paris, France, 1961; p. 183.
22. Hunten, D.M. Spectroscopic studies of the twilight airglow. *Space Sci. Rev.* **1967**, *6*, 493–573. [[CrossRef](#)]
23. Bills, R.E.; Gardner, C.S. Lidar observations of mesospheric Fe and sporadic Fe layers at Urbana, Illinois. *Geophys. Res. Lett.* **1990**, *17*, 143–146. [[CrossRef](#)]
24. Chu, X.; Pan, W.; Papen, G.C.; Gardner, C.S.; Gelbwachs, J.A. Fe Boltzmann temperature lidar: Design, error analysis, and initial results at the North and South Poles. *Appl. Opt.* **2002**, *41*, 4400–4410. [[CrossRef](#)] [[PubMed](#)]
25. Wang, X.; Yi, F.; Huang, K. Double sporadic metal layers as observed by colocated Fe and Na lidars at Wuhan, China. *J. Geophys. Res. Space Phys.* **2017**, *122*, 2237–2248. [[CrossRef](#)]
26. Yi, F.; Zhang, S.; Yu, C.; He, Y.; Yue, X.; Huang, C.; Zhou, J. Simultaneous observations of sporadic Fe and Na layers by two closely colocated resonance fluorescence lidars at Wuhan (30.5° N, 114.4° E), China. *J. Geophys. Res. Atmos.* **2007**, *112*, D04303. [[CrossRef](#)]
27. Yi, F.; Zhang, S.; Yu, C.; Zhang, Y.; He, Y.; Liu, F.; Huang, K.; Huang, C.; Tan, Y. Simultaneous and common-volume three-lidar observations of sporadic metal layers in the mesopause region. *J. Atmos. Sol.-Terr. Phys.* **2013**, *102*, 172–184. [[CrossRef](#)]
28. Alpers, M.; Höffner, J.; Von Zahn, U. Sporadic Fe and E layers at polar, middle, and low latitudes. *J. Geophys. Res. Space Phys.* **1994**, *99*, 14971–14985. [[CrossRef](#)]
29. Chu, X.; Yu, Z.; Gardner, C.S.; Chen, C.; Fong, W. Lidar observations of neutral Fe layers and fast gravity waves in the thermosphere (110–155 km) at McMurdo (77.8° S, 166.7° E), Antarctica. *Geophys. Res. Lett.* **2011**, *38*, L23807. [[CrossRef](#)]

30. Xun, Y.; Yang, G.; She, C.Y.; Wang, J.; Du, L.; Yan, Z.; Yang, Y.; Cheng, X.; Li, F. The first concurrent observations of thermospheric Na layers from two nearby central midlatitude lidar stations. *Geophys. Res. Lett.* **2019**, *46*, 1892–1899. [[CrossRef](#)]
31. Chu, X.; Yu, Z. Formation mechanisms of neutral Fe layers in the thermosphere at Antarctica studied with a thermosphere-ionosphere Fe/Fe+ (TIFe) model. *J. Geophys. Res. Space Phys.* **2017**, *122*, 6812–6848. [[CrossRef](#)]
32. Wang, C.; Xu, J.; Lü, D.; Yue, X.; Xue, X.; Chen, G.; Yan, J.; Yan, Y.; Lan, A.; Wang, J. Construction progress of Chinese meridian project phase II. *Chin. J. Space Sci.* **2022**, *42*, 539–545. [[CrossRef](#)]
33. Xia, Y.; Cheng, X.; Li, F.; Yang, Y.; Lin, X.; Jiao, J.; Du, L.; Wang, J.; Yang, G. Sodium lidar observation over full diurnal cycles in Beijing, China. *Appl. Opt.* **2020**, *59*, 1529–1536. [[CrossRef](#)] [[PubMed](#)]
34. Wang, K.; Wang, Z.; Wu, Y.; Xia, Y.; Xun, Y.; Wu, F.; Jiao, J.; Du, L. Calculation of Resonance Fluorescence Scattering Cross Sections of Metal Particles in the Middle and Upper Atmosphere and Comparison of Their Detectability. *Atmosphere* **2023**, *14*, 1283. [[CrossRef](#)]
35. Li, C.; Wu, D.; Deng, Q.; Cui, F.; Zhong, Z.; Liu, D.; Wang, Y. Simulation and optimization of Fe resonance fluorescence lidar performance for temperature-wind measurement. *Opt. Express* **2022**, *30*, 13278–13293. [[CrossRef](#)]
36. Huang, W.; Chu, X.; Wang, Z.; Fong, W.; Yu, Z.; Smith, J.; Roberts, B. Simultaneous and Common-Volume Lidar Observations of Mesospheric Fe and Na Layers at Boulder: Main Layers, Sporadic Layers, and Meteor Trails. In Proceedings of the AGU Fall Meeting Abstracts, San Francisco, CA, USA, 5–9 December 2011; p. SA51B–1946.
37. Yi, F.; Yu, C.; Zhang, S.; Yue, X.; He, Y.; Huang, C.; Zhang, Y.; Huang, K. Seasonal variations of the nocturnal mesospheric Na and Fe layers at 30 N. *J. Geophys. Res. Atmos.* **2009**, *114*, D01301. [[CrossRef](#)]
38. Nagasawa, C.; Abo, M.; Shibata, Y. Lidar System for Observations of Equatorial Lower and Upper Atmosphere. In Proceedings of the Reviewed and revised papers presented at the 23rd International Laser Radar Conference, Nara, Japan, 24–28 July 2006; pp. 43–46.
39. Gardner, C.S.; Chu, X.; Espy, P.J.; Plane, J.M.; Marsh, D.R.; Janches, D. Seasonal variations of the mesospheric Fe layer at Rothera, Antarctica (67.5 S, 68.0 W). *J. Geophys. Res. Atmos.* **2011**, *116*, D02304. [[CrossRef](#)]
40. Gardner, C.S.; Plane, J.M.; Pan, W.; Vondrak, T.; Murray, B.J.; Chu, X. Seasonal variations of the Na and Fe layers at the South Pole and their implications for the chemistry and general circulation of the polar mesosphere. *J. Geophys. Res. Atmos.* **2005**, *110*, D10302. [[CrossRef](#)]
41. Clemesha, B.R. Sporadic neutral metal layers in the mesosphere and lower thermosphere. *J. Atmos. Terr. Phys.* **1995**, *57*, 725–736. [[CrossRef](#)]
42. Tang, Q.; Zhao, J.; Yu, Z.; Liu, Y.; Hu, L.; Zhou, C.; Zhao, Z.; Feng, X. Occurrence and variations of middle and low latitude sporadic E layer investigated with longitudinal and latitudinal chains of ionosondes. *Space Weather* **2021**, *19*, e2021SW002942. [[CrossRef](#)]
43. Chu, X.; Nishimura, Y.; Xu, Z.; Yu, Z.; Plane, J.M.; Gardner, C.S.; Ogawa, Y. First simultaneous lidar observations of thermosphere-ionosphere Fe and Na (TIFe and TINa) layers at McMurdo (77.84° S, 166.67° E), Antarctica with concurrent measurements of aurora activity, enhanced ionization layers, and converging electric field. *Geophys. Res. Lett.* **2020**, *47*, e2020GL090181. [[CrossRef](#)]
44. Gao, Q.; Chu, X.; Xue, X.; Dou, X.; Chen, T.; Chen, J. Lidar observations of thermospheric Na layers up to 170 km with a descending tidal phase at Lijiang (26.7° N, 100.0° E), China. *J. Geophys. Res. Space Phys.* **2015**, *120*, 9213–9220. [[CrossRef](#)]
45. Nahar, S.N.; Bautista, M.A.; Pradhan, A.K. Electron-ion recombination of neutral iron. *Astrophys. J.* **1997**, *479*, 497. [[CrossRef](#)]

Disclaimer/Publisher’s Note: The statements, opinions and data contained in all publications are solely those of the individual author(s) and contributor(s) and not of MDPI and/or the editor(s). MDPI and/or the editor(s) disclaim responsibility for any injury to people or property resulting from any ideas, methods, instructions or products referred to in the content.